PHYSICAL REVIEW C VOLUME 23, NUMBER 1 JANUARY 1981

Excitation functions for evaporation residues from the ^{37}Cl + ^{169}Tm fusion reaction

W. Schier
University of Lowell, Lowell, Massachusetts 01854

J. Chervenak,* A. C. DiRienzo,† H. Enge, D. Grogan,‡ J. Molitoris,§ M. Salomaa, and A. Sperduto
Laboratory for Nuclear Science, Massachusetts Institute of Technology, Cambridge, Massachusetts 02139

(Received 7 July 1980)

Zero-degree excitation functions of evaporation residues formed primarily by neutron boiloff from the ^{206}Rn compound nucleus in the ^{37}Cl + ^{169}Tm fusion reaction were measured from 148.5 to 186 MeV beam energy. The evaporation residues were identified by their alpha-decay energies. Cross sections associated with $2n$, $3n$, $4n$, $3n\,1p$, $5n$, and $4n\,1p$ emission peak at 155, 157, 165, 168, 177, and 182 MeV, respectively. $3n\,1\alpha$ emission was also observed and shows hints of forward-backward asymmetry. A maximum total evaporation residue cross section of 1.6 ± 0.5 mb was observed at 165 MeV. A comparison of these results to statistical evaporation theory predictions was made, showing fair agreement, except for the $2n$ cross section which was considerably larger than predicted.

[NUCLEAR REACTIONS Complete fusion, ^{37}Cl+ ^{169}Tm, $E = 147$ to 185 MeV lab, excitation functions for evaporation residues.]

I. INTRODUCTION

In heavy-ion reactions producing compound nuclei with $Z > 80$ only a very small fraction of the fusion cross section results in particle boiloff. The great majority of the compound nuclei decay by fission. It is of interest to study such reactions in detail, i.e., to measure the excitation function for the evaporation residues (residual nuclei) produced by emission of 2 neutrons, 3 neutrons, 2 neutrons–one proton, etc. It is hoped that such data may eventually help point the way to the production of super-heavy elements. Computer programs such as ALICE,[1] MB2,[2] or CASCADE[3] can be used for extrapolating cross section data to other target-projectile combinations once the adjustable parameters have been reliably determined. These reactions are also used to produce new nuclides far from the line of stability and to yield new spectroscopic data on known nuclides.

This work is a study of evaporation residue cross sections associated with $2n$, $3n$, $4n$, $5n$, $6n$, $3n1p$, $4n1p$, $3n1\alpha$, and $4n1\alpha$ emission from the ^{206}Rn compound nucleus following the fusion of ^{37}Cl with ^{169}Tm. Excitation functions for these processes were measured at zero degree from 148.5 to 186 MeV beam energy utilizing components of the MIT-BNL energy-mass spectrograph.[4,5] The evaporation residues were identified by the aid of their alpha-decay energies. Angular distributions and velocity distributions were measured at 176 MeV, and the total evaporation residue cross section, integrated over velocity and angle, was determined at that energy.

This reaction also served to test a lifetime measuring procedure that is well suited for evaporation residues which decay by alpha emission or spontaneous fission with half-lives in the range of 10^{-6} to 10 seconds.

II. EXPERIMENTAL METHOD

The MIT-BNL energy-mass spectrograph (EMS), as described in Refs. 4 and 5, consists of a crossed field velocity selector (Wien filter) followed by a modified split-pole spectrograph. Because of its relatively large momentum dispersion it is not a practical instrument when it is desirable to *collect* recoiling evaporation residues for further study. Alternate arrangements of the equipment have therefore been devised. In the present ^{37}Cl + ^{169}Tm fusion reaction, the evaporation residues are formed through particle (primarily neutron) cascades from the ^{206}Rn compound nucleus. The residual nuclei decay predominantly by alpha-particle emission with some competition from electron capture. They are readily identified by their alpha-particle energies. Successive neutron boiloffs give the evaporation residues an angular distribution which is sharply peaked at about zero degree. Proton and alpha-particle boiloff modifies this picture somewhat, as discussed later. However, it is clear that a detection system that offers full rejection of the beam to allow zero degree operation and spacial focusing of the evaporation residues onto a single solid state detector is well suited for this experiment.

The split-pole spectrograph was therefore not used. As shown in Fig. 1, the separation system consists of a modified velocity selector and two magnetic quadrupole doublets. 20-cm long sections of the electrostatic deflector plates have

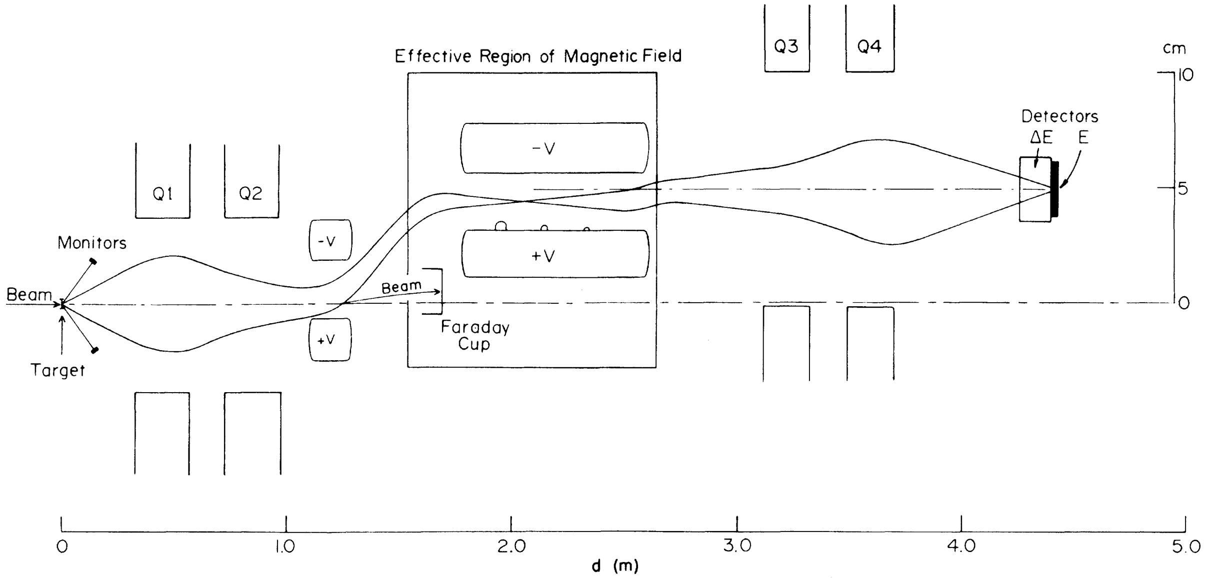

FIG. 1. Beam trap and velocity selector for separation of the beam from evaporation residues at zero degree.

been cut off and mounted separately closer to the target. This effectively separates the main beam from the evaporation residues before these enter the velocity selector proper. The first quadrupole pair produces an image of the target in the middle of the velocity selector, and the second quadrupole pair refocuses this image on the detector. Correct focusing only takes place for the mean charge state and mean velocity of the evaporation residues, and chromatic focusing errors play an important role in the determination of the "effective solid angle" and hence in cross-section calculations (see below).

Beam rejection of the system is excellent. In recent day-long experimental runs, no particles with energies higher than those of the evaporation residues (≈30 MeV) were recorded, indicating that the rejection of beam particles above 30 MeV is better than 1 part in 10^{15}. In the range 6 to 30 MeV a few background events, possibly produced by beam particles, were recorded. The device does, however, allow the passage through the system, at zero degree, of some (typically 200 sec^{-1}) low-energy scattered beam particles with velocity comparable to that of the fusion products, i.e., with energies of approximately 5 MeV.

The fusion products embed themselves in the solid state detector and subsequently decay, primarily by alpha emission. If the alpha particles are stopped in the depletion layer, they give rise to full energy peaks. However, since the range of the alphas is approximately 5.6 times greater than the average range of the evaporation residues, about 43 percent of the alphas, emitted largely in the backward direction, escape through the surface of the detector. Hence, about 57 percent of the particles deposit the full energy in the detector. The rest are registered as a background of lower-energy events, mostly at energies far below the lowest-energy alpha peak. Only the events in the peaks could be identified, and a correction factor of 1/0.57 was applied in the cross-section calculations.

The low-energy beam tail referred to above does interfere to a certain extent with the low-energy part of the alpha spectrum. In order to eliminate this background, a ΔE gas detector was installed in front of the E detector for the latest exposures. The ΔE detector created an anticoincidence gate completely eliminating the beam background.

The detector system was energy calibrated with an ^{241}Am alpha source and the electronics tested for linearity with a pulser. Energy shifts of the calibration peak due to dead layers on the detector and source surfaces were studied by orienting each separately at 60° to the normal of the other. The total effect produced a 30-keV shift in the peak energy. Since the alpha decay in the present experiment takes place inside the depletion layer of the detector, the recoil of the alpha daughter also contributes to the pulse height. The recoil energy is about 130 keV, but because of the large pulse height defect at these energies, only a small fraction is observed in the pulse height. The pulse height defect was estimated from a graph published by Haines and Whitehead[6] to be about

86% of 130 keV, leaving 18 keV as a contribution. With this correction included, the measurements of alpha energies in this work agree with published values[7,8] to better than ±10 keV. Because of the uncertainties involved in the correction, we are, in this paper, adopting the published values rather than our own.

Although half-lives of the evaporation residues formed in the present study are well known, the reaction was also employed as a test of a method for lifetime measurements. In this procedure, the evaporation residue pulse simultaneously started a multiscaler and triggered an electrostatic deflector that cut off the beam. Data was recorded in a 2-D time vs energy mode. The beam was held off for a duration equal to several half-lives of the parent nuclide. Although this is not an optimal way to obtain lifetime information when the fusion product count rate is high and lifetimes are greater than several seconds, the method is very well suited for measuring short half-lives when the counting rate is low. The flight time through the system is of the order of 1 μsec, so this sets the lower limit for such lifetime measurements.

The evaporation residue cross section was obtained at 176 MeV by measuring both velocity profile at zero degree and angular distribution of individual evaporation residues. The velocity distribution is measured by varying the ratio of the electric field to magnetic field. All fields are varied in a precalculated fashion assuming constant mass m but a mean charge state $\bar{q}$ that varies with velocity in a known fashion. Folded into the results of such measurements is the velocity-acceptance function of the instrument. This function was determined as follows.

When the electric and magnetic fields of the device are set for particles of given m, v, and $\bar{q}$, the effective solid angle for these particles is determined simply by geometry. For other velocities and/or mass to charge ratios, the effective solid angle rapidly diminishes because of the selectivity of the velocity selector and because of chromatic focusing errors. These effects have been calculated[9] with the program RAYTRACE.[10] We have also determined the effective solid angle experimentally in the following way. A gold beam with energy 33 MeV, roughly matching that of the evaporation residues, was elastically scattered from a thin gold target and detected in the separator, which was set at an angle of 21.8°. This angle is the same as the angle of the two surface-barrier monitor detectors. The ratio of counting rates then directly gives the effective solid angle of the device relative to the solid angle of the monitors. The elastically scattered gold particles have a sharp velocity spectrum but the charge state distribution is approximately the same as for the evaporation residues. By varying the electric-to-magnetic field ratio, a velocity profile is produced (Fig. 2). Each point represents the effective solid angle integrated over the charge state distribution for a sharp velocity. To determine the total cross section for evaporation residue formation one needs to measure the velocity distribution and unfold the result with use of the acceptance function shown in Fig. 2. The ^{169}Tm target thickness was approximately 400 μg/cm^2. At this thickness the velocity spread caused by energy degradation of the fusion products in the target is comparable to the velocity acceptance of the system. The thick target also contributes considerably to the width of the measured angular distribution because of multiple scattering.

III. EXPERIMENTAL RESULTS

Figure 3(a) shows a spectrum of alpha particles from evaporation residues embedded in a 600 mm^2 surface-barrier detector. Part of the spectrum is obscured by the low-energy beam particles that make it through the system. In Fig. 3(b) is shown the same spectrum taken with a 450 mm^2 detector (better resolution) and in anticoincidence with the gas ionization counter.

Figure 4 is a simplified section of the Chart of Nuclides[7] with the alpha lines observed in this work. As mentioned earlier, the alpha energies

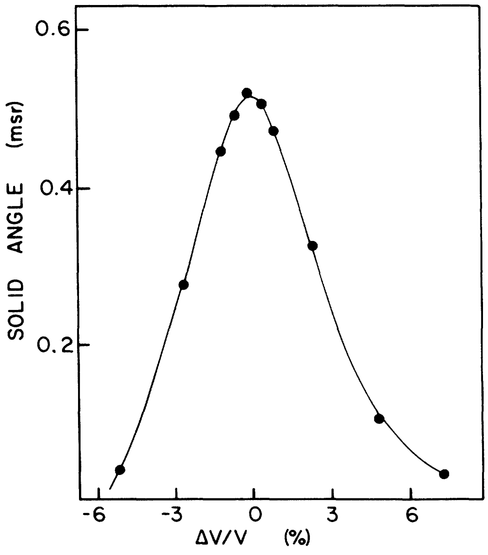

FIG. 2. Effective solid angle vs velocity measured with elastically scattered ^{197}Au ions with an energy of 28.5 MeV at $\theta = 21.8°$.

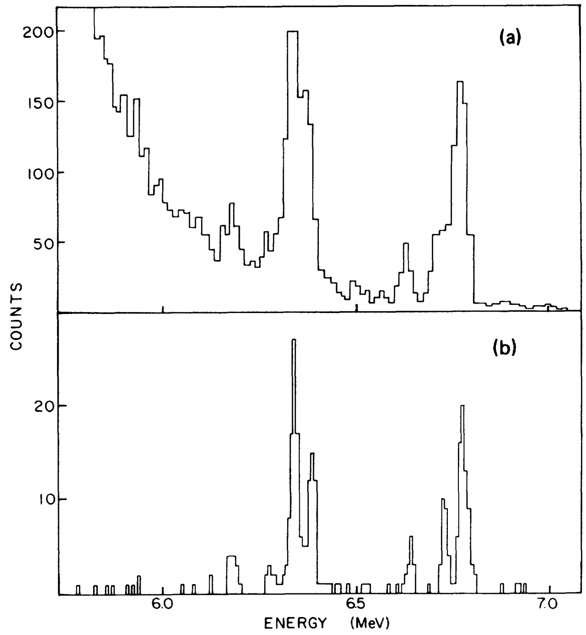

FIG. 3. Alpha spectra from evaporation residues imbedded in the *E* detector (a) 600 mm^2 detector (b) 450 mm^2 detector with ΔE anticoincidence.

quoted here are taken from the *Table of Isotopes*.[8]

The character of the alpha particle spectrum changes notably with increasing beam energy as the number of evaporated particles changes and new nuclides are formed. Parent and daughter alpha group intensities resonate in unison with changing beam energy.

Figure 5(a) shows excitation functions for parent alphas observed with the apparatus at zero degree and with the velocity selector adjusted to accept particles with velocities centered about the velocity of the compound nucleus. As explained further below, this practically excludes evaporation residues from reactions such as $3n1\alpha$, in which a *prompt* alpha particle is emitted, because the nucleus then recoils out of the acceptance momentum space of the apparatus.

Most of the nuclides produced in the reaction studied have half-lives of less than one min. In hour-long exposures we therefore also observe the alpha-emitting daughter nuclides. Figure 5(b) shows excitation functions for the daughters. A comparison between the intensities of the daughter lines and parent lines yields directly the alpha branching ratio for the daughter nuclides, provided the "daughter" is not also created as an evaporation residue in an $xn1\alpha$ reaction, i.e., with a prompt alpha particle emitted at the target position rather than in the detector. This contribution is made negligibly small by making branching ratio measurements near the peak in the excitation function of the parent (since the prompt alpha process with the same number of neutrons peak approximately 10 MeV higher in incident beam energy) and at the velocity of the center-of-mass (since the evaporation residues associated with prompt alphas gives a negligible contribution here). The published alpha branching ratios for all the nuclei identified are listed in Table I, and those measured in the present experiment are listed for the daughters. The agreement between our measure-

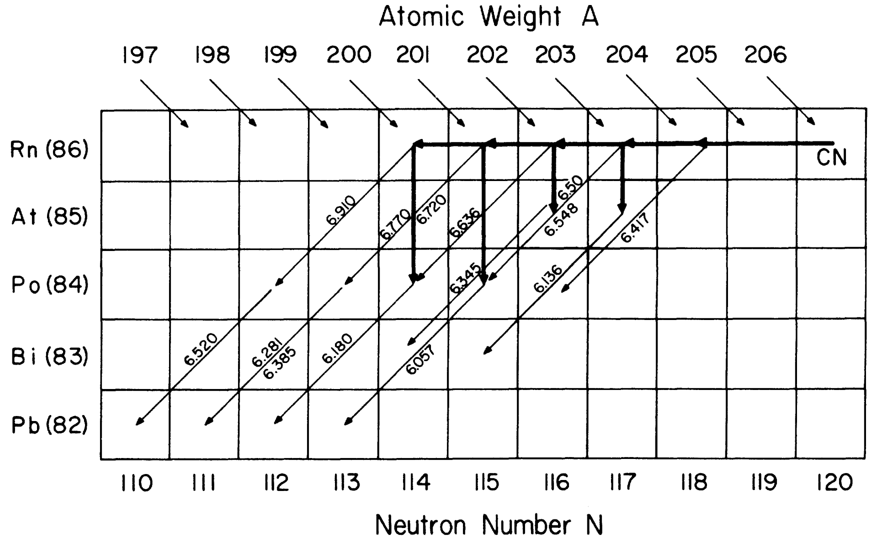

FIG. 4. Part of the Chart of Nuclides showing evaporation modes (heavy lines) and alpha lines observed in this work (light lines).

TABLE I. Alpha branching ratio values in this and previous experiments.

Nucleus	E_α (MeV)[a]	Alpha branching ratios Present	 Previous	Source
^{200}Rn	6.91		0.98[b]	Ref. 12
^{201}Rn	6.72		0.80[b]	Ref. 12
^{201}Rn^m	6.77		0.90[b]	Ref. 12
^{202}Rn	6.636		<0.70[b]	Ref. 12
			0.85 ± 0.15	Ref. 13
^{203}Rn	6.500		0.66 ± 0.09	Refs. 12 and 14
^{203}Rn^m	6.548		(1.00)	Ref. 12
^{204}Rn	6.417		0.70 ± 0.02	Ref. 12
^{201}At	6.345		0.71 ± 0.07	Ref. 15
^{202}At	6.136		0.15 ± 0.03	Ref. 15
			0.12 ± 0.008	Ref. 16
^{196}Po	6.520		0.95[b]	Ref. 12
^{197}Po	6.281	0.44 ± 0.07	0.9 ± 0.1	Ref. 12
^{197}Po^m	6.395	0.84 ± 0.09	0.85[b]	Ref. 12
^{198}Po	6.180	0.63 ± 0.02	0.70 ± 0.08	Ref. 12
^{199}Po^m	6.057	0.41 ± 0.05	0.39 ± 0.04	Ref. 12
			0.275 ± 0.02	Ref. 15

[a] Energies were taken from the Chart of the Nuclides, Ref. 7.

[b] β-strength function systematics from Ref. 11 were used for estimating the partial β half-lives in Ref. 12.

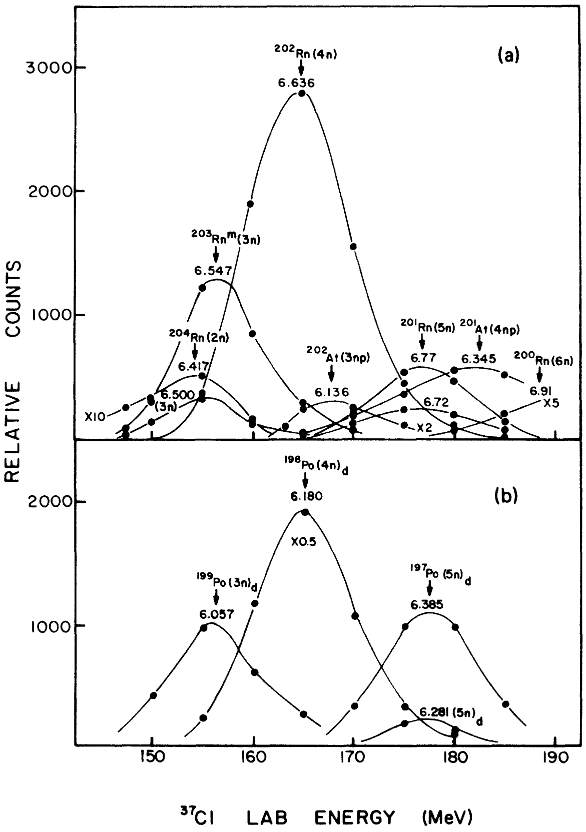

FIG. 5. Excitation functions of alpha lines seen in transitions from (a) parent nuclei and (b) daughter nuclei.

ments and published data is generally good, except for the case of ^{197}Po, for which we measure a branching ratio for alphas of 0.44 ± 0.07, whereas the published value is 0.9 ± 0.1.

Representative theoretical velocity distributions and angular distributions of evaporation residues from the ^{37}Cl + ^{169}Tm fusion reaction calculated with the kinematic code BETH[17] are shown in Figs. 6 and 7, respectively. There are distinct differences in the shapes of the velocity and angular distributions depending upon if the reaction proceeds via xn, $xn1p$, or $xn1\alpha$ evaporation. These distribution shapes are quite helpful in identifying new nuclear species. The measured velocity and angular distributions will be somewhat less distinct due to target thickness effects (energy loss, straggling, and multiple scattering) and due to the roughly 6-percent width of the velocity acceptance function of the separator system (Fig. 2).

Figure 8 shows measured velocity profiles at a beam energy of 176 MeV. All velocity distributions have been normalized to the same peak height for shape comparison (with the exception of the $3n1\alpha$ case, which is normalized at half the peak height). The $4n$ (6.36 MeV alpha), $5n$ (6.720), and $5n^*$ (6.770) cases are displayed in Fig. 8(a) with the daughter distributions shown directly below in Fig. 8(c) [$4n_d$(6.180), $5n_d$(6.280), and $5n_d^*$(6.385)]. The dashed curve plotted through the $4n$ data points in Fig. 8(a) is redrawn in Fig. 8(c) normalized at the peak point. The

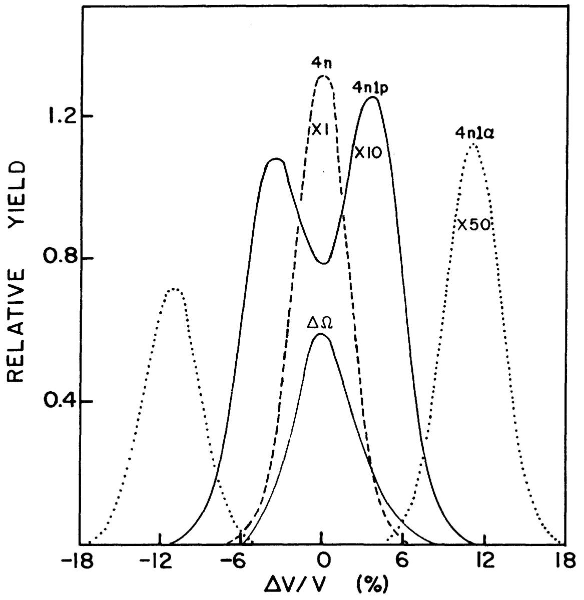

FIG. 6. Velocity spectra of evaporation residues as predicted by the kinematics program BETH. Superimposed is the resolution function for the recoil-mass selector (Fig. 2).

difference between the 6.180 MeV data points and the dashed curve are the two dotted bell-shaped curves. Comparison with Fig. 6 shows that the 6.180 data have to be interpreted as a superposition of alpha yield from the 4*n* daughter on the yield from the identical nuclide (^{198}Po) produced directly by 4*n*1*α* evaporation.

The 5*n* and 5*n** data points and those of their daughters approximately follow the 4*n* velocity profile (dashed curve), although the 5*n* distributions appear to be somewhat narrower. Figure 8(b) is a good example of 4*n*1*p* (6.345) distribution. Although the curve in this figure connects the 4*n*1*p* data, the 3*n*1*p* (6.136) data points, having considerably greater statistical uncertainty, essentially follow the same velocity profile. Figure 8(d) is the 3*n*1*α* (6.057) velocity distribution, an exampleof a cascade including an alpha particle without a superimposed daughter profile obscuring it, as in the 4*n*1*α* case.

Figure 9 shows angular distributions measured at 176 MeV and normalized at 0° for shape comparison. Each data point consists of a sum over the velocity distribution at that angle. The placement of the distributions are identical in Figs. 8 and 9 and the same point and line symbols are used for the data and curves in these figures. Here again one observes characteristic shapes for pure neutron cascades, with one proton and several neutrons and cascades with one alpha and several neutrons. The 5*n* and 5*n** distributions and those of their daughters fall off more rapidly than the 4*n* distribution. When the dashed curve for the 4*n* distribution is multiplied by the alpha branching ratio of the 5*n* daughter and subtracted from the 6.180 MeV alpha data, the dotted angular distribution for the 4*n*1*α* cascade remains [see Fig. 9(c)]. The 4*n*1*p* and 5*n*1*p* angular distributions are, within experimental errors, identical as were their velocity profiles, and both are broader than those from the pure neutron cascades. Error bars assigned to the angular distribution data are also representative of uncertainties associated with the velocity profile data.

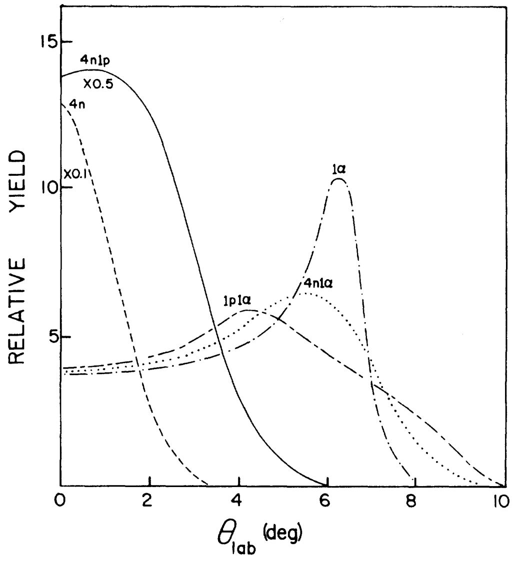

FIG. 7. Angular distributions, integrated over velocity as predicted by the kinematics program BETH.

To check that parent alpha branching ratios (which cannot be measured in the present experiment) are essentially correct and that the formation of non-alpha emitting evaporation residues was negligible, a comparison can be made between parent alpha counts and evaporation residue counts. The parent alpha counts are corrected both for their branching ratios and the 1/0.57 solid-angle factor and then summed. Part of the data included in the analysis was taken before the anticoincidence counter was installed, and the counts were, of course, then also corrected for the beam tail background. Figure 10 shows the results of this comparison. A curve has been drawn through the data points (circles) for the evaporation residues. The corrected summed parent alpha counts (square symbols) are observed to closely follow the same curve. The error bars arise primarily from branching ratio uncertainties. The evaporation residue

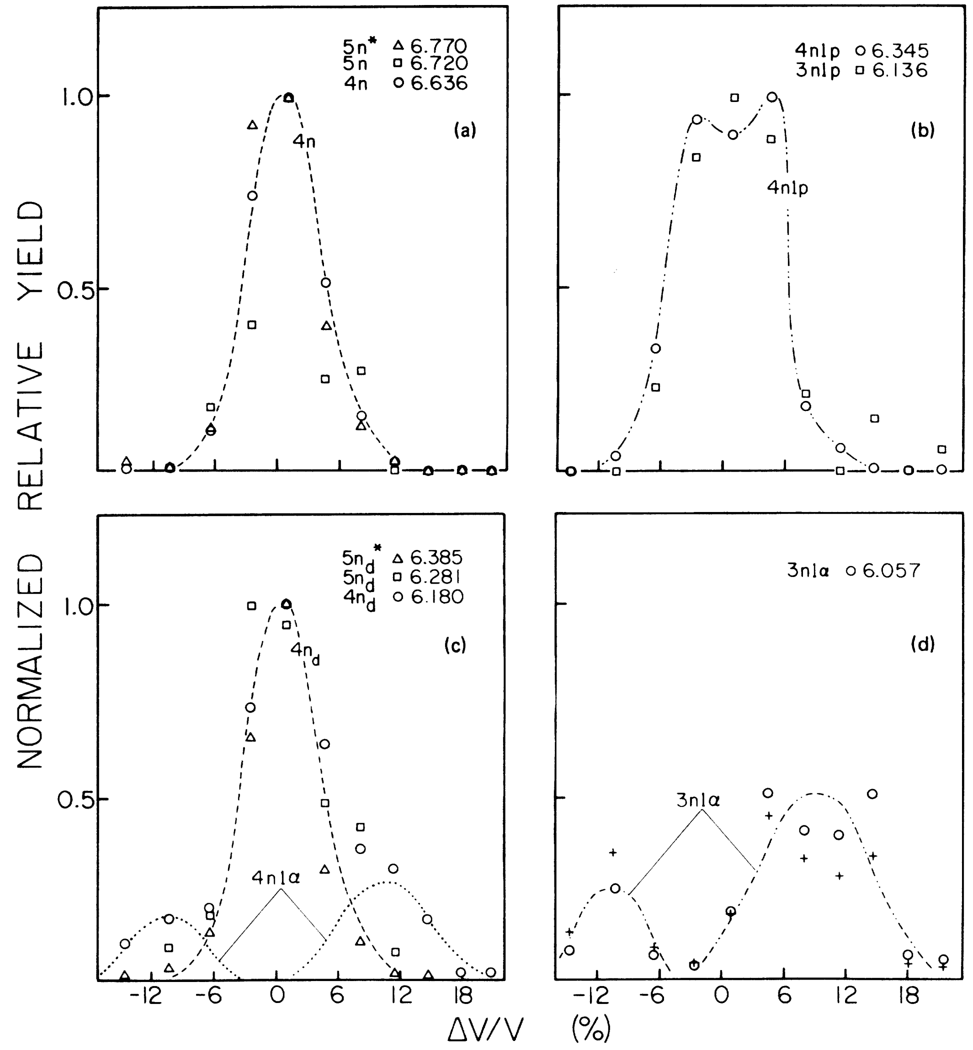

FIG. 8. Velocity distributions of evaporation residues in the laboratory system. The yields are normalized to unity at $\Delta v/v = 0$ for intercomparison. Characteristic error bars are as in Fig. 9. In the $3n1\alpha$ case the circles represent laboratory cross sections and the crosses center-of-mass cross sections.

counts may include a small contribution of ^{169}Tm nuclei knocked out of the target by 180° elastic scattering of the lower-energy ^{37}Cl in the beam "tail." Such "background" events are estimated from a comparison run of ^{37}Cl on ^{197}Au to be less than 10% of the measured evaporation-residue counting rate in the present experiment.

Experimental absolute cross sections for the evaporation residues from the $^{37}\mathrm{Cl} + {}^{169}\mathrm{Tm}$ fusion reaction are presented in Fig. 11 as solid curves. These cross sections are obtained by integrating the angular distributions of the parent alphas, correcting for the branching ratios and the 1/0.57 factor, and utilizing the solid angle versus velocity for the recoil-mass selector RMS system (Fig. 2). Excitation functions of absolute cross sections are derived from the $\theta = 0°$ and $\Delta v/v = 0\%$ excitation functions normalized to an absolute cross section scale at 176 MeV. This procedure is valid since the velocity and angular distributions do not change appreciably over an individual excitation function. The dashed curves are evaporation residue cross sections calculated with the ALICE program. These calculations will be discussed in the following section. Since excitation functions do not exist for the $3n1\alpha$ and $4n1\alpha$ cases, the shapes of these functions as drawn in Fig. 11 (solid curves) are determined from the theoretical curves at 176 MeV, where data exist. In the normalization procedure, one also relies on the fact that elastic scattering of ^{37}Cl from ^{169}Tm is predominantly Rutherford scat-

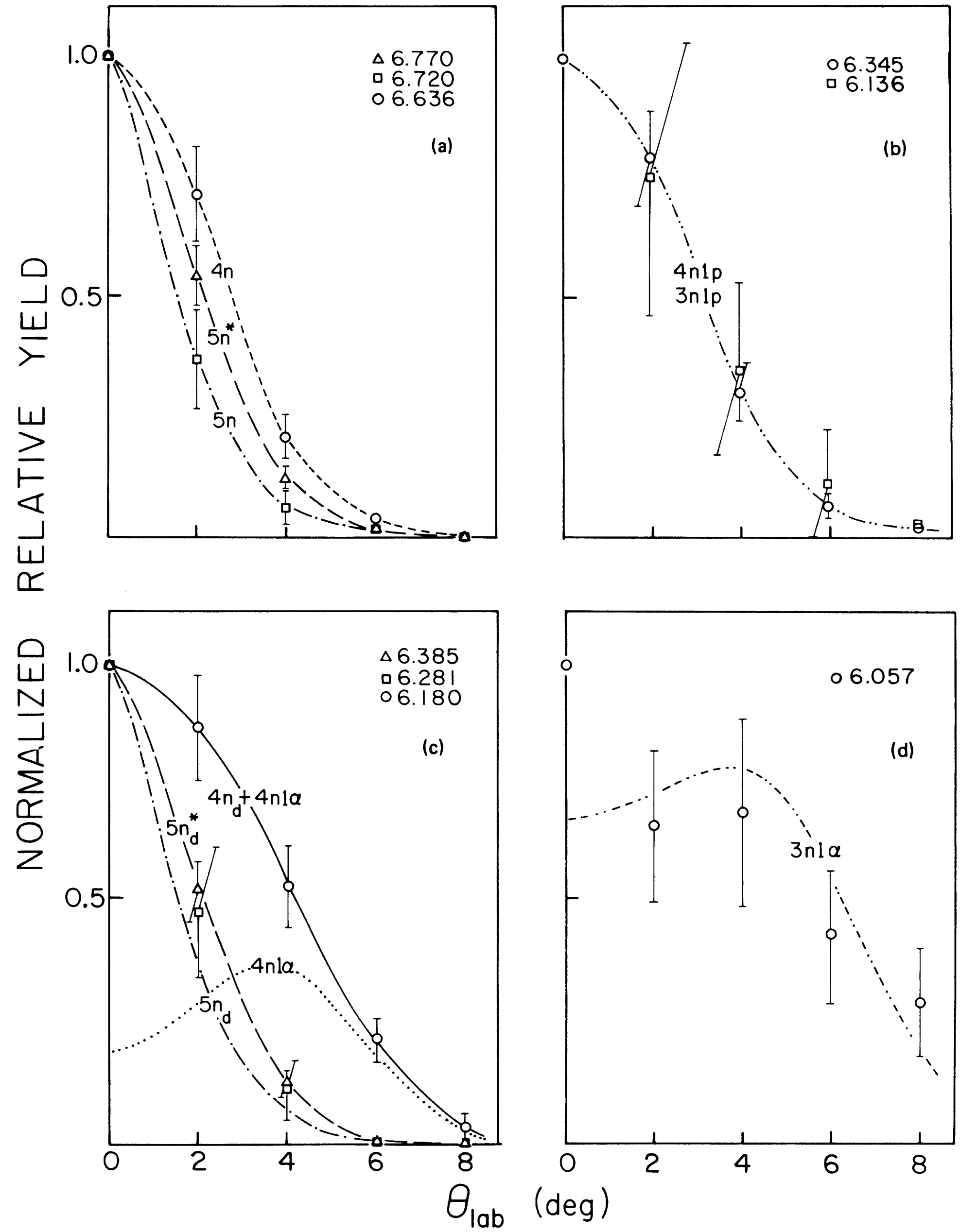

FIG. 9. Angular distributions of evaporation residues integrated over velocity. The symbols are the same as in Fig. 8.

tering at the 21.8 degree angle of the monitors.

By summing the individual excitation functions, the total evaporation residue cross section in Fig. 12 is obtained. At the optimum beam energy, 165 MeV, the 1.6-mb cross section represents only about 0.2% of the total (calculated) cross section. The rest of the compound nuclei presumably fission.

Figure 13 shows results of timing measurement made for one alpha line in accordance with the procedure described in the previous section. The straight line represents a half-life of 9.9 sec, which is the same as the published value.

IV. DISCUSSION

The nuclides produced in this work have all been observed earlier by other authors. The alpha energies measured are in agreement with earlier work and so are the alpha branching ratios

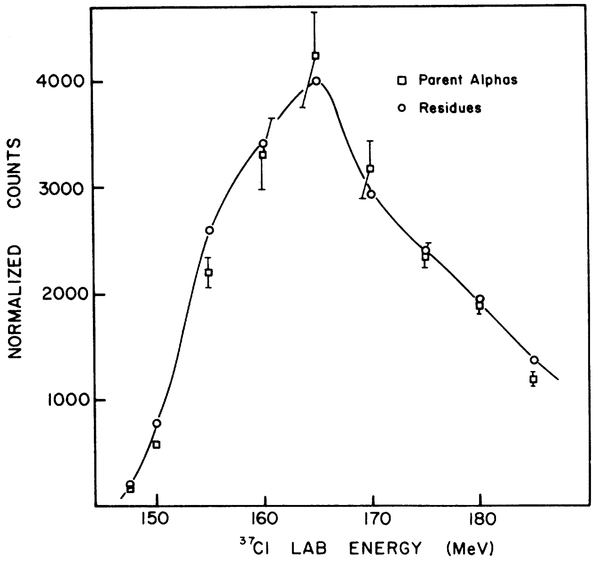

FIG. 10. Comparison between alpha decay counts, corrected for counter efficiency and alpha branching ratio, and the counts of evaporation residues.

except in one instance: the ratio for ^{197}Po is 0.44 ± 0.07, in disagreement with the value 0.9 ± 0.1 quoted on the Chart of Nuclides. In the present work the nuclei are imbedded in the active volume of the solid state detector and the measurements are recorded over many half-lives of parent and daughter. The ratio is measured directly as a ratio of alpha yields from ^{197}Po, the daughter, and from ^{201}Rn, the parent. Direct formation of the daughter by $5n1\alpha$ emission is virtually excluded because the measurements were made at zero degree and at the central velocity and at a beam energy that substantially enhanced $5n$ production over $5n1\alpha$ production. The only substantial errors in the quoted ratio are therefore the statistical ones.

The principal reason for studying this reaction was to obtain information about the fusion process in this region of the nuclidic chart, particularly the survival from fission. The results have been compared with the computer code ALICE, even though more sophisticated codes were available to us (but more expensive to run). We are basically using the code to determine the breakup branches $3n$, $4n$, $3n1p$, etc., that survive fission. In the present study, presumably, only relatively low-angular momentum compound states contribute to the evaporation residue cross section, so correct accounting for angular momentum as is done in the more sophisticated codes is not extremely important.

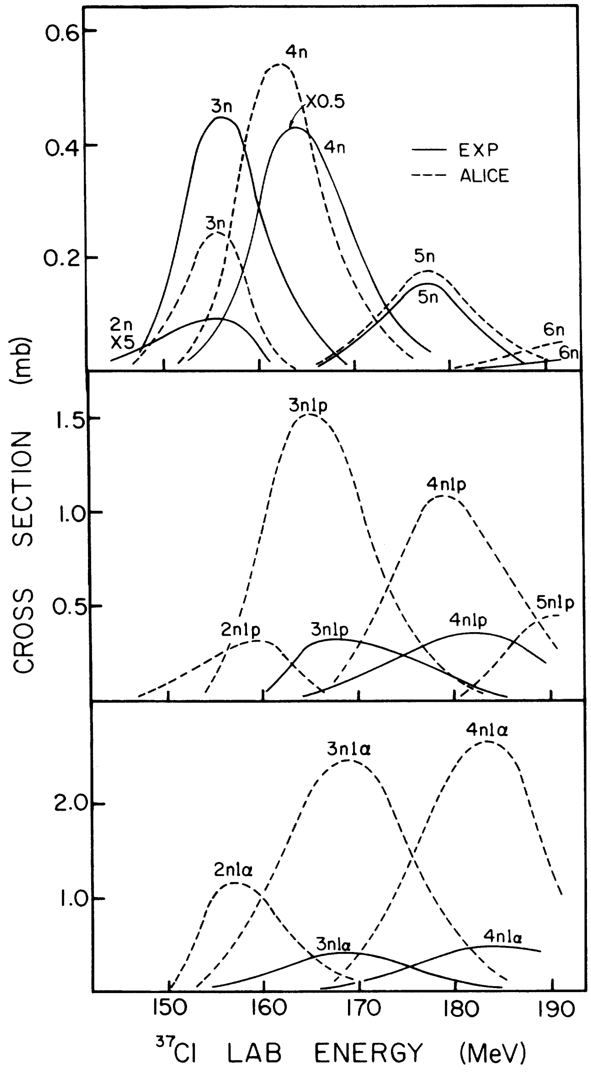

FIG. 11. Comparison between excitation functions as measured and as calculated with the evaporation code ALICE.

The most glaring discrepancies between the experimental results and the ALICE calculations are the stronger experimental preference for the xn breakups than for the $xn1p$ and $xn1\alpha$ breakups (Fig. 11). With our choice of adjustable parameters for ALICE, the calculated $3n$, $4n$, and $5n$ cross sections are within a factor of 2 of the observed ones and generally on the low side. For the $xn1p$ and $xn1\alpha$ reactions the calculated cross sections are generally a factor of 5 too high. Only the relative cross sections are meaningful because a slight change in the adjustable parameters (e.g., the fission barrier) will change all the calculated absolute cross sections substantially.

Another difference between experiment and calculations is the systematic trend of experimental

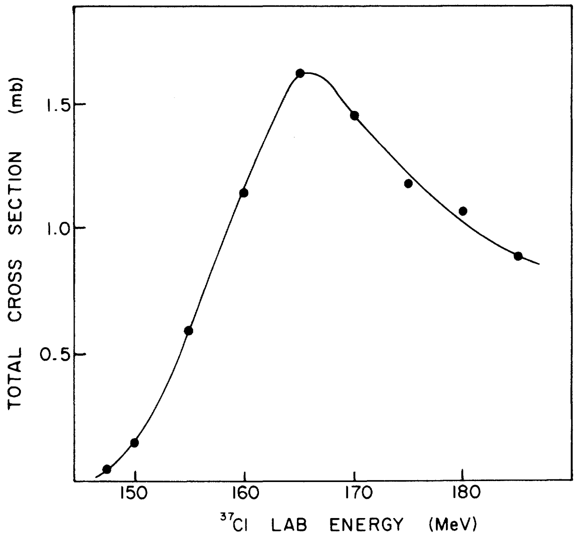

FIG. 12. Total evaporation-residue cross section for the reaction ^{37}Cl+ ^{169}Tm.

enhancement of the few-neutron cross section, in particular the $2n$ cross section. With the chosen parameters the calculated value for $\sigma(2n)$ at the peak (151 MeV) is 0.24 μb, whereas the measured value at the peak (155 MeV) is 18 μb. The excitation energy of the compound nucleus at $E_b = 155$ MeV is 43.1 MeV and the sum of the binding energies of the two first neutrons is 17.5 MeV, leaving 25.8 MeV to be shared between neutron kinetic energy and gamma rays. Presumably all compound states with high angular momenta decay by fission. The yrast energy for the states that decay by $2n$ emission is therefore quite low. Each of the two neutrons emitted need to have a kinetic energy of almost 8 MeV in order to leave the system within 10 MeV of the yrast line. This is far out on the tail of neutron evaporation spectra. Using standard semiempirical formulas[17] for such spectra, one finds that the probability for evaporation of an 8-MeV neutron is 2 orders of magnitude lower than the probability for evaporation of a 1-MeV neutron (near the maximum). These arguments and, of course, more quantitatively, the disagreement with the ALICE calculations, do raise some serious questions about whether or not the compound nucleus is equilibrated before the emission of these neutrons.

As mentioned earlier, the angular distributions of the $5n$ residues are significantly narrower than the $4n$ distributions (Fig. 9). This may at first glance be puzzling, but may actually only be reflecting the fact that, since the excitation energy of the compound nucleus is fixed, more kinetic energy is carried away by the four neutrons than

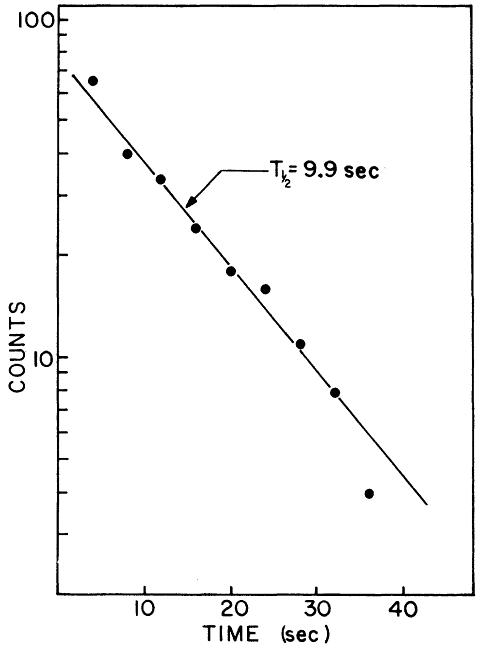

FIG. 13. Lifetime measurement for the nuclide ^{202}Rn.

by the five neutrons. Indeed, assuming isotropy, the width of the angular and velocity distributions, corrected for atomic effects in the target, is a measure of the average total kinetic energy carried away by the neutrons.

There is also a probable difference between the widths of the $5n$ and $5n^*$ distributions. This may be taken as a somewhat inconclusive evidence that the formations of ^{201}Rn and ^{201}Rn^m follow different gamma ray cascades already from the start, since the excitation energies after neutron boiloff presumably are different. If the neutrons are emitted from the compound nucleus isotropically, one should see a similar difference in the zero-degree velocity distributions. This difference appears to be less significant (Fig. 8), hinting that the $5n$ distribution is more forward-backward peaked than the $5n^*$ distribution. This does not alter the tentative conclusion about different gamma-ray paths.

In an earlier communication from this group[18] we have shown a hint of forward-backward asymmetry [in the center-of-mass system (cms)] of the residues recoiling from an $xn\alpha$ evaporation. When corrected for kinematic effects the $4n1\alpha$ reaction [Fig. 8(c), dotted curve] does not show such an asymmetry, however, the $3n1\alpha$ reaction does. The circles in Fig. 8(d) are experimental points, uncorrected for kinematic effects. The crosses represent relative cross section in center-of-mass units. There is some evidence of asymmetry, but, again, because of the poor statistics, the evidence is not conclusive.

The reaction is the first of a series that we have studied involving ^{37}Cl and heavy target nuclei. The evaporation-residue cross sections for these reactions decrease very rapidly with Z^2/A. For the most neutron-rich target nuclei, the cross section decreases by about a factor of 6 for each unit of Z^2/A. This does not give much promise for superheavies produced by heavy-ion fusion although it should be noted that of all the combinations of stable or semistable nuclei that can be fused to form the compound nucleus ^{206}Rn, the combination chosen here leaves the compound nucleus at the highest excitation energy when fusion takes place at the Coulomb barrier.[20] In other words, it is a poor choice if the objective is to produce a "cold" compound nucleus.[21]

ACKNOWLEDGMENTS

This work was supported by the U.S. Department of Energy under Contract No. AC02-76ER03069. The authors wish to thank Dr. G. Young for his assistance in setting up the timing electronics.

---

*Present address: Mission Research Corp., P.O. Box 1209, La Jolla, Calif. 92038.

†Present address: U. S. Military Academy, West Point, N.Y. 10996.

‡Present address: U. S. Army, Germany.

§Present address: Stanford University, Stanford, Calif. 94305.

[1] M. Glann, Report No. COO-3494-29 1976 (unpublished); Report No. COO-3494-32, 1976 (unpublished); OVERLAID ALICE descriptions and revisions.

[2] M. Beckerman and M. Blann, University of Rochester, Report No. UR-NSRL-135A, 1977.

[3] F. Pühofer, Nucl. Phys. A280, 267 (1977).

[4] H. A. Enge and D. Horn, Nucl. Instrum. Methods 145, 277 (1977).

[5] M. Salomaa and H. A. Enge, Nucl. Instrum. Methods 145, 271 (1977).

[6] E. L. Haines and A. B. Whitehead, Rev. Sci. Instrum. 37, 190 (1966).

[7] Chart of Nuclides, Twelfth Edition, Knolls Atomic Power Laboratory, Schenectady, N.Y.

[8] *Table of Isotopes*, 7th ed., edited by C. M. Lederer and V. S. Shirley (Wiley, New York, 1978).

[9] S. B. Kowalski and H. A. Enge, RAYTRACE (unpublished).

[10] A. C. DeRienzo, M. S. thesis, Massachusetts Institute of Technology, 1980.

[11] C. L. Duke, P. G. Hansen, O. B. Nielsen, and G. Rudstam, Nucl. Phys. A151, 609 (1970).

[12] P. Hornshøj, K. Wilsky, P. G. Hansen, A. Lindall, and O. B. Nielsen, Nucl. Phys. A163, 277 (1971).

[13] K. Valli, M. J. Nurmia, and E. K. Hyde, Phys. Rev. 159, 1013 (1967).

[14] P. Hornshøj (private communication) (revised α branching ratio of 0.45 ± 0.08 to value 0.66 ± 0.09).

[15] P. Hornshøj, P. G. Hansen, and B. Johnson, Nucl. Phys. A230, 380 (1974).

[16] R. M. Latimer, G. E. Gordon, and T. D. Thomas, J. Inorg. Nucl. Chem. 17, 1 (1961).

[17] C. Bolton, W. Schier, N. Tsoupas, H. Enge, M. Salomaa, A. Sperduto, and A. Graue, Phys. Rev. C 18, 293 (1978); C. Bolton, M. S. thesis, University of Lowell, 1978 (unpublished).

[18] D. Horn, H. A. Enge, A. Sperduto, and A. Graue, Phys. Rev. C 17, 118 (1978).

[19] A. DiRienzo, H. Enge, D. Grogan, J. Molitoris, S. Sperduto, M. Salomaa, W. Schier, and W. Wegner, Bull. Am. Phys. Soc. 25, 522 (1980).

[20] H. Wegner, W. Schier, H. Enge, A. DeRienzo, A. Sperduto, M. Salomaa, and S. Gazes, Bull. Am. Phys. Soc. 25, 522 (1980).

[21] J. Huizenga and A. Ghiorso, cited in V. E. Viola, Jr. and B. D. Wilkins, Nucl. Phys. 82, 65 (1966).